EARTHQUAKE ENGINEERING AND STRUCTURAL DYNAMICS
Earthquake Engng. Struct. Dyn. **28**, 1273–1294 (1999)

STATISTICAL STUDY OF SPATIAL VARIATION OF RESPONSE SPECTRUM USING FREE FIELD RECORDS OF DENSE STRONG MOTION ARRAYS

HIDEJI KAWAKAMI*† AND SHAILENDRA SHARMA‡
Department of Civil and Environmental Engineering, Saitama University, Urawa, 338-8570, Japan

SUMMARY

Spatial variation of acceleration response spectra is examined using strong motion records for a large number of events from dense accelerometer arrays at Chiba in Japan and SMART-1 in Lotung, Taiwan. The effects of earthquake component, structural damping, earthquake magnitude, focal depth, epicentral distance, structural time period, and station separation on the intra-event variation of response spectra are examined first through an empirical analysis and then through a least-square regression fit for parametric study. A very large scatter of the response spectra ratio is observed for both arrays, especially for SMART-1 array. The mean values of the ratio vary from 10 to 20 per cent for Chiba array while they vary from 25 to 50 per cent for SMART-1 array. The coefficients of variation of the ratio range from 5 to 25 per cent for Chiba array and 30 to 50 per cent for SMART-1 array. The correlation among response spectra is found to be inversely proportional to station separation and shows frequency dependence. For larger time periods, the correlation is lower and not higher. The correlation is also lower for UD earthquake component as compared to the two horizontal components. For higher damping ratio, the correlation among spectra is higher. The effect of the earthquake magnitude, focal depth and epicentral distance on the spatial variation is complex. The three parameters having implicit interdependence, considering their combined effect, a positive contribution to the value of ratio of response spectra is observed in the case of larger earthquake events. Furthermore, as mentioned above, the spatial variation for SMART-1 array is much larger than that for Chiba array. This difference can be attributed mainly to the difference in distance between the instruments in the two arrays. However, some of the difference is considered to be due to site specific characteristics.

KEY WORDS: spatial variation; response spectrum; dense instrument arrays; statistical study; regression analysis

1. INTRODUCTION

It has been noted in a large number of post earthquake field surveys of damage that for any earthquake event, the degree of damage suffered by similar structures varies appreciably from one

* Correspondence to: Hideji Kawakami, Department of Civil and Environmental Engineering, Saitama University, 255 Shimo-Okubo, Urawa-shi, Saitama 338-8570, Japan.
† Professor
‡ Graduate Student

Received 26 September 1998
CCC 0098–8847/99/111273–22$17·50 *Revised 21 April 1999*

Accepted 28 May 1999

location to another, even though the separation between two structures may be reasonably small. This variation seems to be caused by differences in ground motion. In structural design based on the reliability theory, the variance of earthquake force is as important as the mean value itself. For long-span structures and embedded lifeline structures as well, the spatial variation of response acceleration has important implications. Therefore we attempt to examine the spatial variation of earthquake damage potential statistically. The acceleration response spectrum has been used as an indicator of the damage potential as it reflects both the effect of amplitude as well as frequency content of the ground motion.

Strong motion records from 39 events for Chiba array in the University of Tokyo, Japan and 40 events for SMART-1 array, in Taiwan having a range of magnitudes, epicentral distances and focal depths have been considered. Response analysis is carried out for discrete structural time periods of 0·1, 0·2, 0·5, 1·0 and 2·0 sec. For an earthquake event, the ratio of ordinates of acceleration response spectra for a certain time period, for any station pair, reflects the spatial variation in response over the separation distance.

Even when we consider intra-event variation only, there is appreciable change in response acceleration amplitudes among stations, although two sites are more or less uniform. To identify the causal factors, regression analysis is used for both the arrays with ratio of response spectra as criterion and station separation, structural time period, damping coefficient, magnitude, epicentral distance, focal depth and earthquake components as variables.

1.1. Chiba array system[1]

The Chiba dense array system located about 30 km east of Tokyo as shown in Figure 1, became operational in April, 1982. At that time, there were 11 bore holes; C0–C4 and P1–P6. Four other bore holes (P7–P9 & P0) were added in January, 1985. The instruments used are piezo-electric-type acceleration transducers with practically flat sensitivity between 0·1 and 30 Hz. Sets of three accelerometers in the three principal directions have been installed at GL -1, -5, -10, -20 and -40 m in different bore holes. In this study, we have considered only the free field records from GL -1 m level. In plan, eight bore holes are densely arranged around the bore hole C0. Bore holes C1–C4 are only 5 m from C0 and P1–P4 are each 15 m from C0. There is a larger triangular network P0-P8-P5 with the bore holes at the three vertices of the triangle.

The topographical and geological conditions of the Chiba site are generally simple. The ground surface is almost flat with little variation in surface profiles from one station to another. The top 3–5 m of the site is covered with loam having SPT values less than 10. This is underlain by a sandy clay layer 2–4 m thick again with SPT values less than 10. Below this is a diluvium sand layer with SPT values more than 20–30 and stiffness increasing with depth. Overall, the soil structure is relatively simple. As measured by down hole shooting method, the P-wave velocity is 0·32 km/s in the loam, 0·55 km/s in the sandy clay layer and 1·67 km/s in the diluvium sand layer. Ground water table is lower than GL -5 m. A complete description of the array system and site conditions has been given by Katayama, Yamazaki *et al.*[2]

1.2. SMART-1 array system[3]

The SMART-1 strong motion array is located in the north east corner of Taiwan near the city of Lotung on the Lan-Yang plain as shown in Figure 2. The array started operating in 1980. The

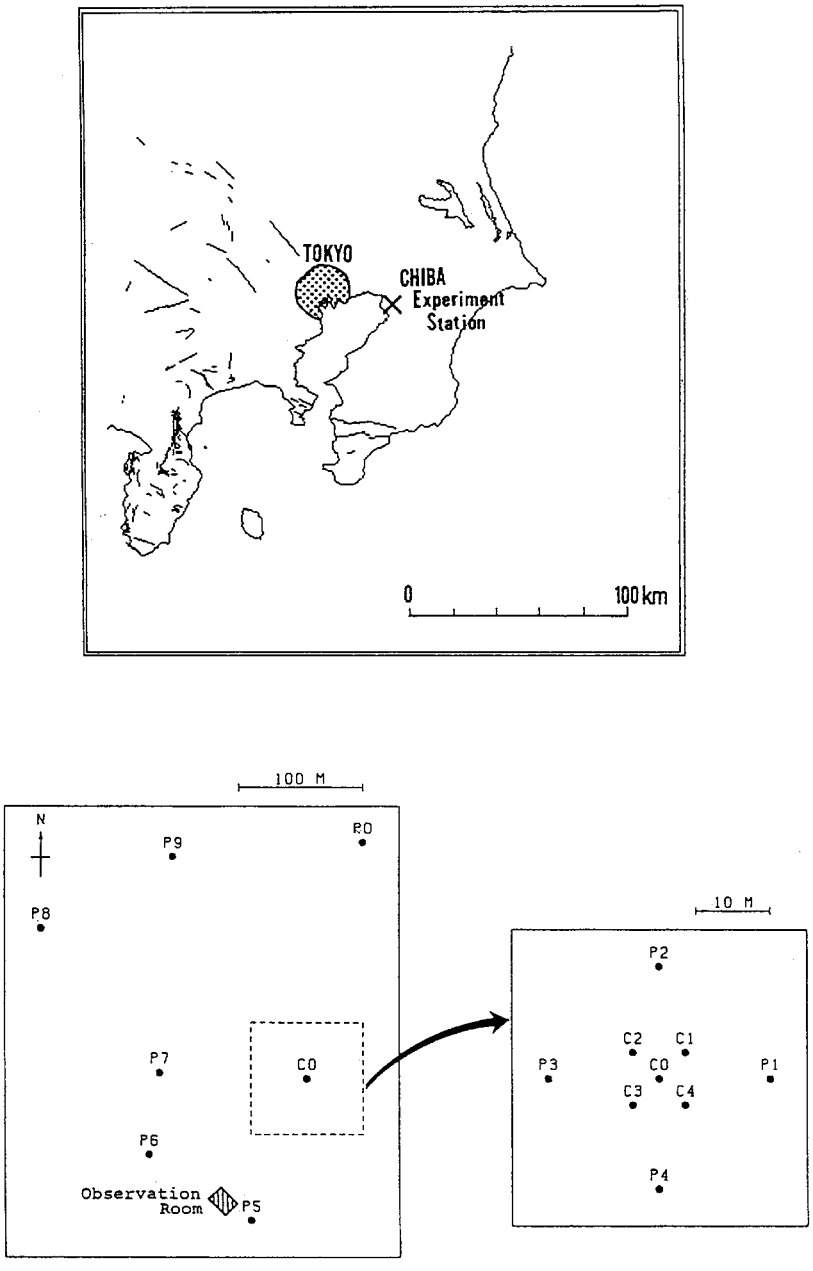

Figure 1. Location of Chiba array and layout of bore holes (after Katayama *et al.*[1])

installation of instruments was completed in August 1982. At that time, the array consisted of 37 force balanced triaxial accelerometers arranged in three concentric rings of radii 200, 1000 and 2000 m with one station C-00 at the centre. Each of the three rings had 12 equally spaced stations numbered clockwise from north direction as I-01 to I-12 (Inner ring), M-01 to M-12 (Middle ring)

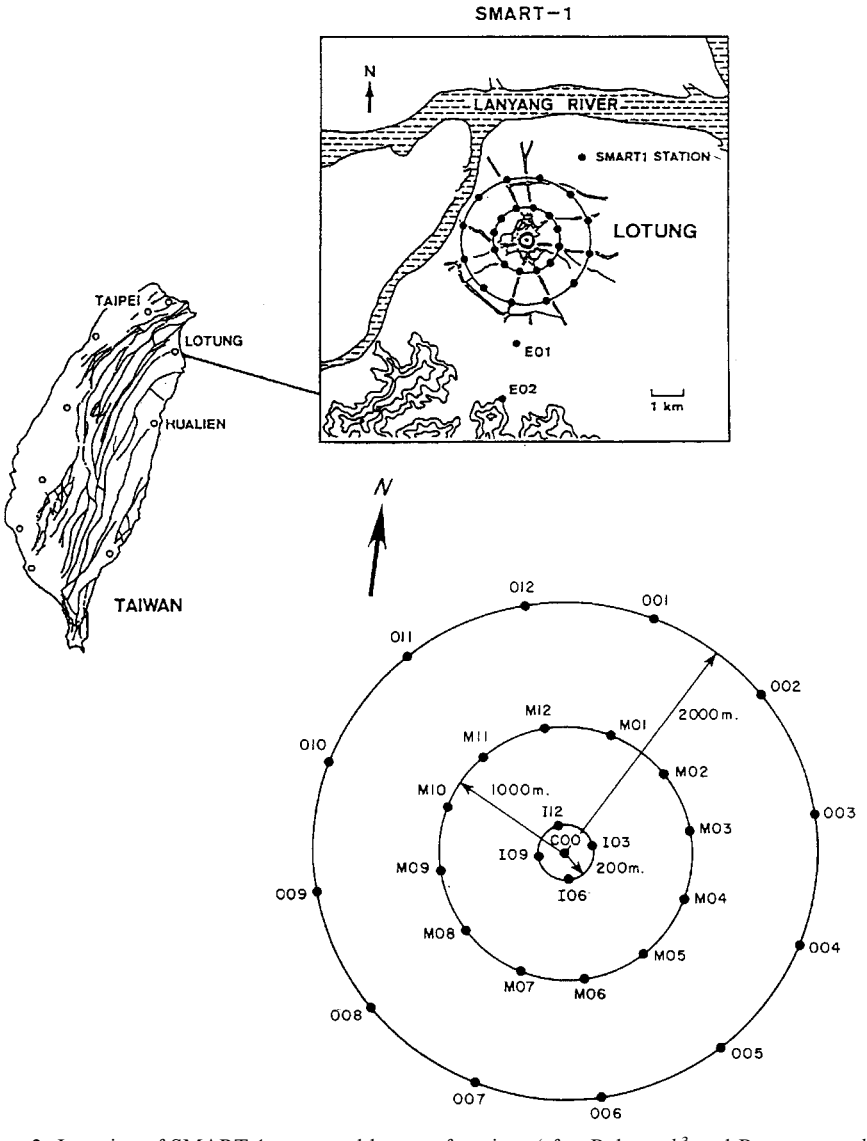

Figure 2. Location of SMART-1 array and layout of stations (after Bolt *et al.*[3] and Beresnev *et al.*[4])

and O-01 to O-12 (Outer ring). Later on, in June 1983, two more stations, E-01 and E-02 were added. These are located 2·8 and 4·8 km south, respectively, from the central station C-00. All the instruments are SA-3000 triaxial accelerometers, having a natural frequency of approximately 80 Hz. A more complete description of array configuration and instrumentation has been given by Bolt *et al.*[3] Any variations due to structure interface and embedment have been minimised since all of the devices are free field instruments mounted on 4 in thick concrete base mats, approximately 2×3 feet across.

The instruments in this array are located on soil sites in a recent alluvial plain except the station E-02 which is on a slate rock outcrop. The top soil is 2·4–18·1 m of grey sandy silt and silty sand across the array. This is followed by some gravel over recent alluvium, to a depth of 30–60 m. Below is a layer of 170–540 m thick deposit of Pleistocene gravels. The basement consists of Miocene Lushan formation slate, sloping gently to the north-north east direction at about 6°. The P-wave velocity is in the range 0·43–0·70 km/s in the top soil, 1·4–1·7 km/s in the recent alluvium, 1·8–2·0 km/s in the Pleistocene and 3·3–4·0 km/s in the Miocene basement.[5] The Lushan formation depth below the SMART-1 array varies from GL -390 to -450 m west to east and GL -180 to -600 m south to north. The detailed profiles of subsurface structure are available.[3,6] As such, the subsurface geology is fairly homogeneous. The ground water table is very high, almost at ground level, the location being close to the mouth of Lan-Yang river.

2. STATION-WISE MEAN OF RESPONSE SPECTRA

As a first step, the response spectrum ordinates for discrete time periods of 0·1, 0·2, 0·5, 1·0 and 2·0 sec were calculated stationwise. The structural damping ratio was taken as 0·10 and records analysed for each earthquake component, one event at a time. Then the mean value was calculated at every station over all the events to check for any bias in the response among the various stations of each array.

2.1. Chiba array

For the three earthquake components, a total of 1338 free field strong motion records from 39 events taking place between 23 July, 1982 and 6 March, 1989 were considered. For the EW component and a structural damping ratio of 0·10, the stationwise mean of response spectra ordinates for all the events calculated at discrete time periods is shown in Figure 3. The plot shows a uniform response over the array for each component except in case of stations P8, P9 and P0. These three stations show a larger variation. Upon closer scrutiny, it was found that there are only three events for which data for P8-P0 stations at GL-1 m level are available. Also, if only these three events are considered for all stations, the mean values for all the stations are comparable. Since we have calculated ratios of response accelerations component-wise and in intra-event terms in our further analysis, the above variation is not likely to have any distorting effect on the results.

The stations show the highest mean response acceleration for 0·2 sec time period. Generally the response acceleration reduces for larger time periods from 0·2 to 2·0 sec and above for both EW and NS components. This indicates the existence of high spectral peaks around 0·2 sec time period for most of the ground motion records.

2.2. SMART-1 array

In all, 40 events taking place between 18 Oct. 1980 and 14 Nov. 1986 were considered. These were, event no. 1–5 and 11–45 as listed by the National Geophysical Data Center, Boulder, USA for Taiwan Earthquakes, SMART-1 array.[7] Considering all the three earthquake components, 2917 free field strong motion records are analysed. The mean values of response spectra for all the events are shown in Figure 4 for the EW component.

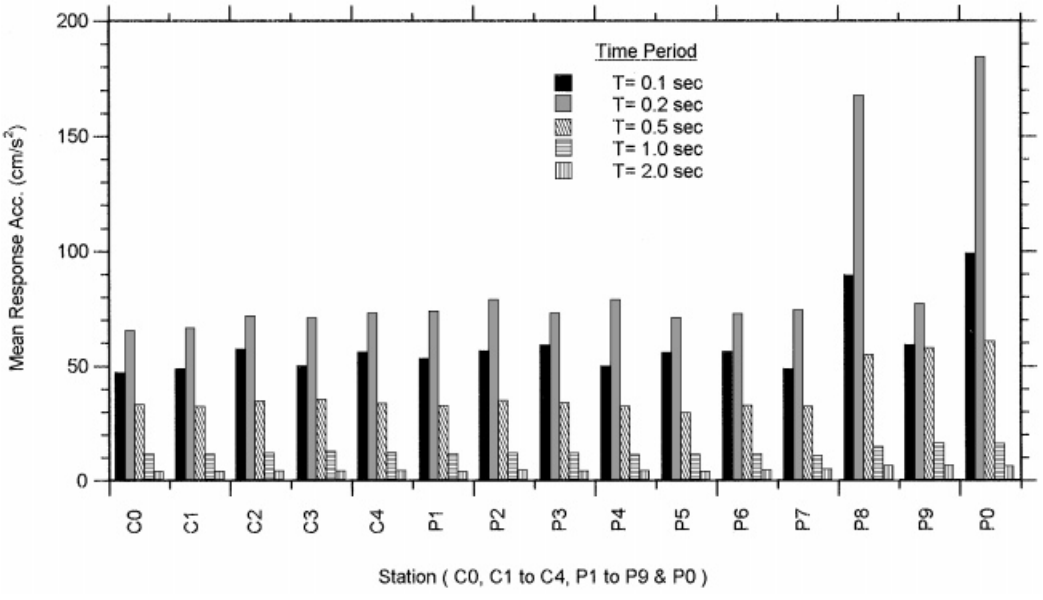

Figure 3. Mean response acc. at each station for different time periods — Chiba array, EW-component

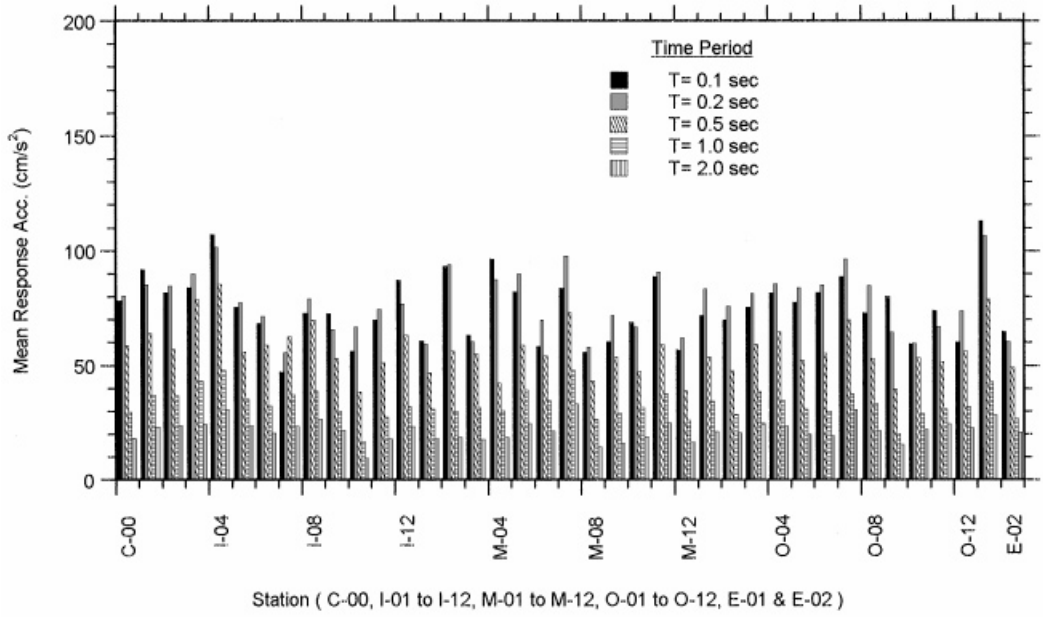

Figure 4. Mean response acc. at each station for different time periods — SMART-1 array. EW-component

The variation of mean spectra for SMART-1 array with the time period is similar to Chiba array although the range of variation from station to station is larger. The natural period of vibration, T, of independent soil columns under SMART-1 has been estimated; Centre station

(C-00), $T = 1{\cdot}1$–$1{\cdot}4$ sec, southern edge (station O-06–O-07) $T = 0{\cdot}7$–$0{\cdot}9$ sec, northern edge (station O-12–O-01) $T = 1{\cdot}5$–$2{\cdot}0$ sec.[5] However, Figure 4 does not reflect the variation one would expect from the gradual variation in soil column depth discussed above. Schneider *et al.* studied a number of dense arrays and observed that a slight shift in resonance across a site can easily generate large variations in amplitude at a given frequency.[8] Bolt *et al.* noted that the standard normalised pseudo-acceleration response spectra for SMART-1 array had shapes which correlated best with the average spectra for hard site conditions and that this was not consistent with the relatively soft site conditions of the array.[3] They attributed it to dominant influences from the source mechanism.

Among different time periods in Figure 4, the highest mean response acceleration at various stations generally corresponds to 0·2 sec time period. Generally the response is lower with increasing period for time periods larger than 0·2 upto 2·0 sec for the horizontal earthquake components.

3. PROBABILITY DENSITY FUNCTION OF SPECTRAL ORDINATE RATIO

To study the spatial variation of response spectra, the ratios of spectral ordinates at a time period for all possible combinations of stations in an array were calculated for each event and then analysed statistically. The ratios were calculated as (smaller value)/(larger value) for all station pairs rather than taking the response of any one station as the base response. Apparently, the closer the values of the ratio are to 1, the higher is the correlation among the two concerned spectral ordinates.

Since most structures have the damping ratio in the range of 0·05–0·20, two values of the damping ratio, viz. 0·10 and 0·20 were used in this study in order to examine its effect on response spectra ratio. Scatter plots were then made for each component and for each time period separately using these two damping ratio values.

The typical scatter plots for the EW component with a 0·10 damping ratio as well as 0·1, 0·5 and 2·0 sec time periods are shown in Figure 5 for Chiba array and in Figure 6 for SMART-1 array. It can be readily seen that there is a very large scatter in the results, especially for SMART-1 array, and that the spectra ratios in Chiba array tend to be higher than those for SMART-1 array. While the values of response spectra ratio in the case of Chiba array are generally higher than 0·6 and not lower than about 0·3 for any case, for SMART-1 array, a reasonable number of spectra ratio values can be observed as low as 0·1 or less. It can also be seen in Figure 5 that the scatter plots shifts towards higher values of response spectra ratio for change of time period 0·1–0·5 sec.

To analyse the distribution of spectral ordinate ratio with station spacing and structural time period, the probability density function is calculated from the scatter plots for various station separation ranges, considering ratio increments of 0·05. These values are then plotted against the mean ratio of each ratio range. For Chiba array, the station separation ranges are 0–40 m, 40–160 m, and larger than 160 m. In case of SMART-1 array, the station separation ranges were 0–650 m, 650–1600 m, 1600–2400 m, 2400–3200 m, 3200–4200 m, 4200–5100 m and larger than 5100 m.

3.1. Chiba array

The typical plots of probability density function of spectral ratios for Chiba array EW component records are shown in Figure 7, respectively, for structural time periods 0·1, 0·5 and

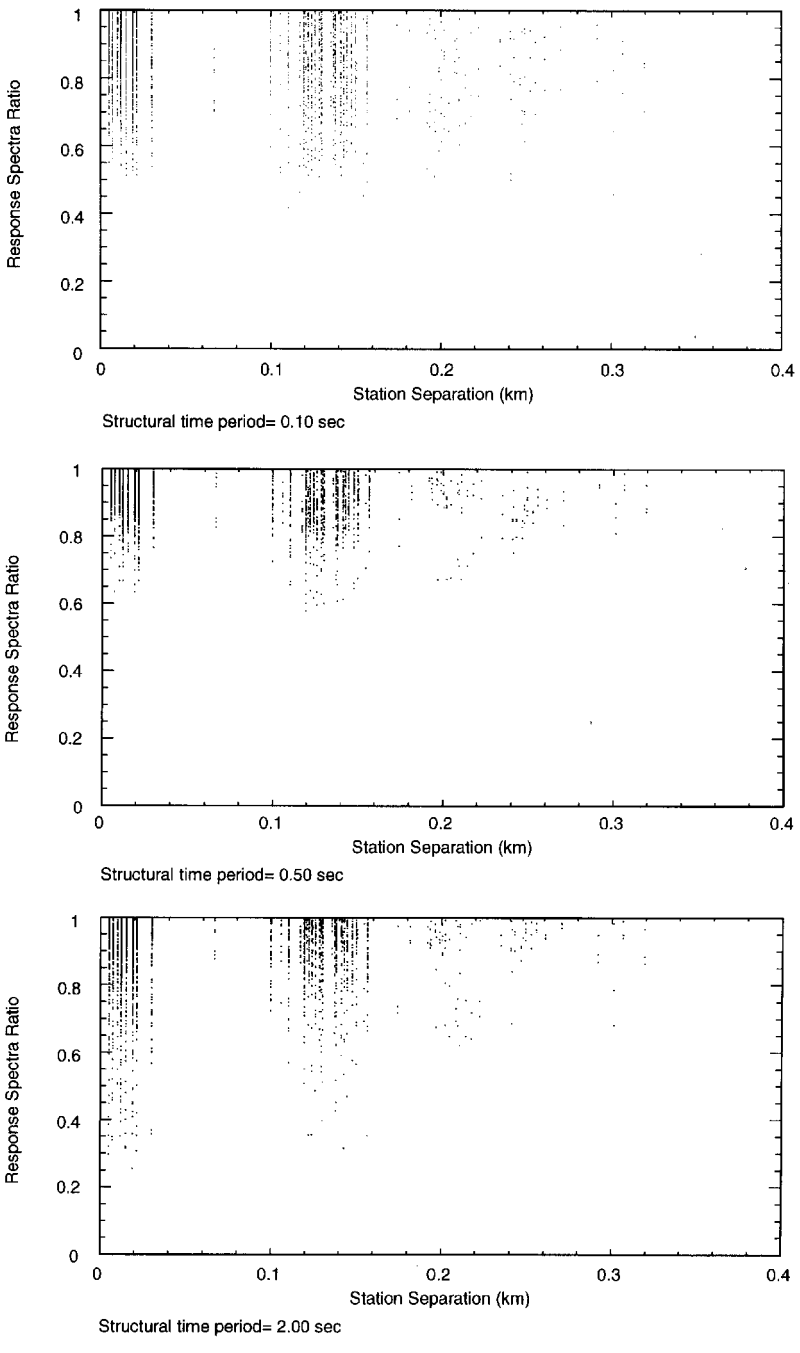

Figure 5. Scatter plot of response spectra ratio vs. station separation for Chiba array, EW-component, damping = 0·10

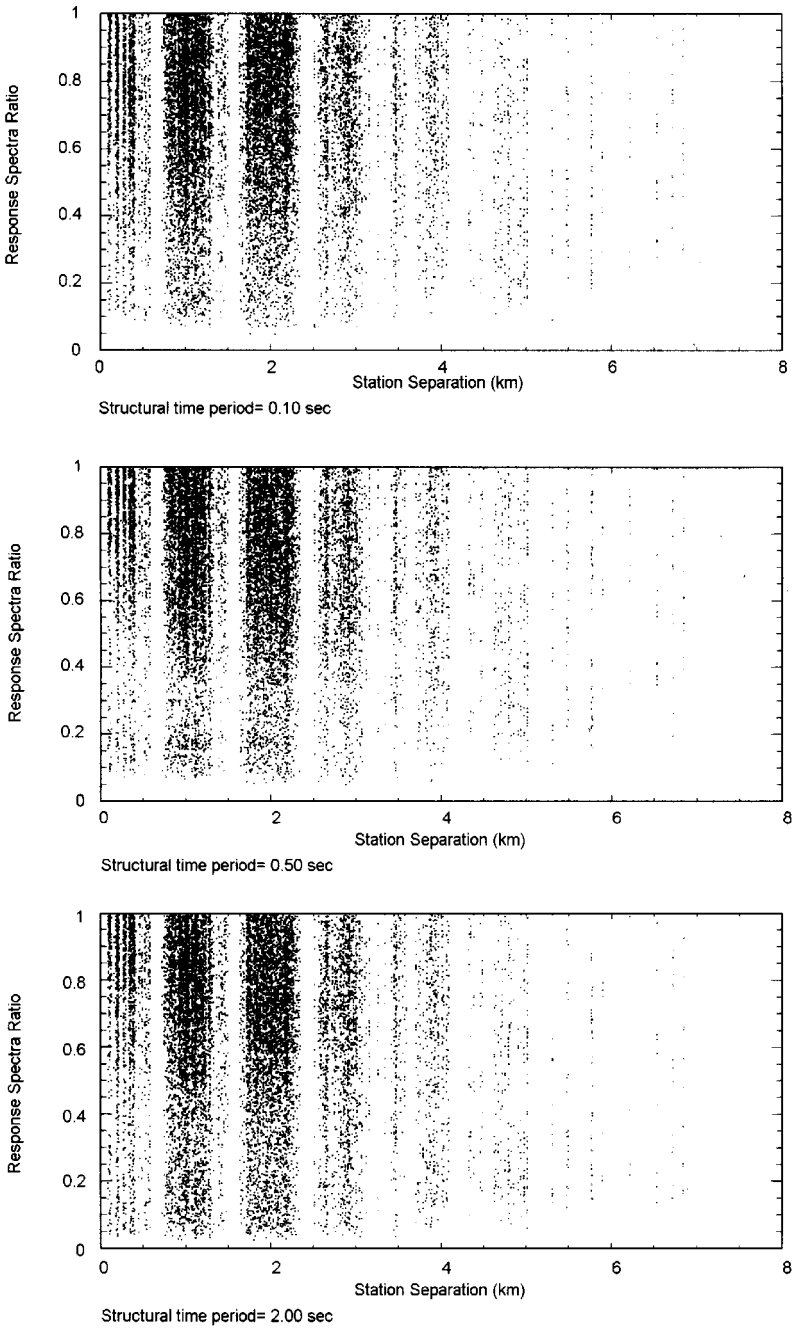

Figure 6. Scatter plot of response spectra ratio vs. station separation for SMART-1 array, EW-component, damping = 0·10

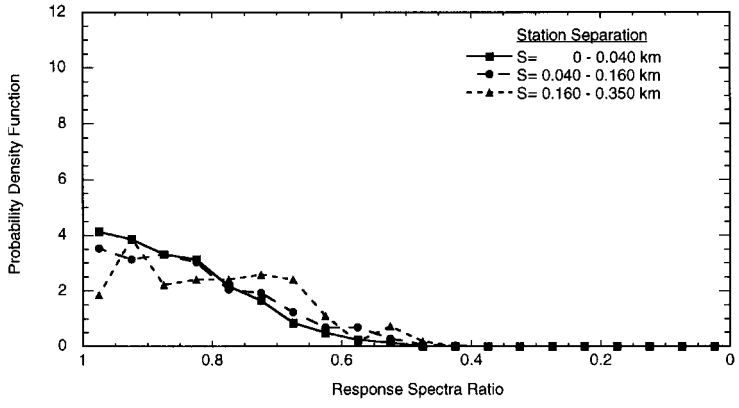

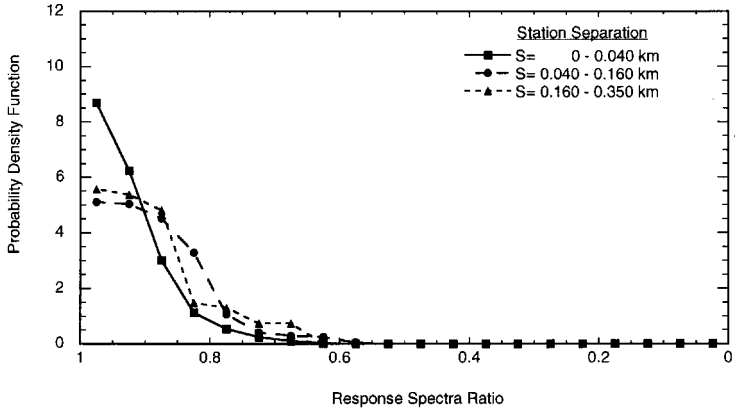

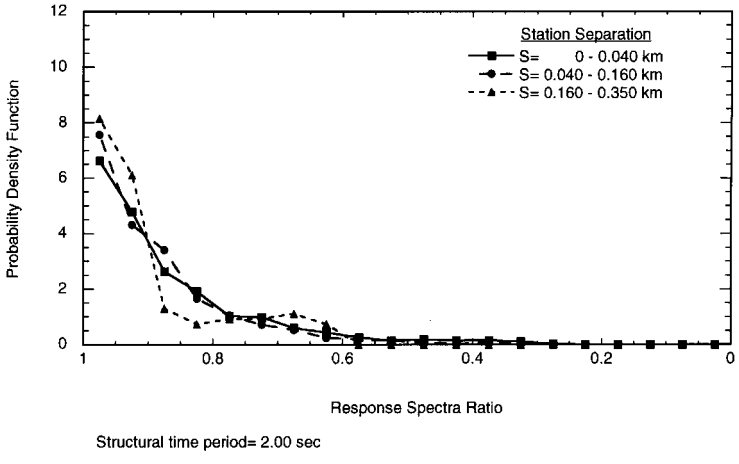

Figure 7. Probability density function for different station separation ranges for Chiba array, EW-component, damping = 0·10

2·0 sec with 0·10 damping ratio. Following are the observations:

(1) Peaks at the highest ratio range (1·00–0·95) are clear for almost all the cases, for all components and for all the three station separation ranges considered. The highest probability achieved is therefore still for the case when the spectral ordinates are nearly equal. If we had not constrained the ratios to be calculated as (smaller value) /(larger value) for the station pairs, we would get a probability density function plot symmetrical about the axis ratio $= 1{\cdot}0$.

(2) There is an inverse relationship between ratio of acceleration response spectra and station separation. For each time period, the probability density function plots show the highest peaks for the shortest station separation range except for large time periods larger than about 2·0 sec. As station separation increases, the peaks become lower and the curves generally flatter, indicating the reduction in correlation among spectral ordinates.

(3) The probability density function is frequency dependent. For the high-frequency region around 0·1 sec period, probability density function is almost unchanged over the ratio range 0·8–1·0. The overall maximum probability density function for all distance ranges is observed for the structural time periods 0·5–2·0 sec. The higher peaks near the higher ratio end reflect the higher correlation among response spectra in statistical terms.

3.2. SMART-1 array

The typical probability density function plots for the EW component records of SMART-1 for structural time periods 0·1, 0·5 and 2·0 sec with 0·10 damping ratio are shown in Figure 8. The following observations are made:

(1) Compared to Chiba array, the probability density function plot against response spectra ratio is flatter. This indicates a generally lower correlation among response spectra for SMART-1 than for Chiba array. This is attributable mainly to larger station separation for SMART-1 array while site specific effects also have their contribution.

(2) There is an inverse relationship between ratio of response spectra and station spacing. The curve for the shortest station separation range (S = 0–0·650 km) shows a general shape which is different from curves for larger spacings and similar to Chiba curves. As station separation increases, the peaks of probability distribution become lower and the curves generally flatter, reflecting the reduction in correlation among spectral ordinates.

(3) The probability density function for various station separation ranges shows frequency dependence.

4. STATISTICAL MEAN OF RATIO OF SPECTRAL ORDINATES

From the probability density function curves that are drawn for each structure time period, the statistical mean and the coefficient of variation of the spectral ordinate ratio can be worked out. The plots of the statistical mean and the coefficient of variation of the spectral ordinate ratio against the structural time period are shown in Figures 9(a) and (b) for Chiba array and SMART-1 array. It can be inferred from these plots that

(1) The ratio of response spectra ordinates has a clear inverse relation with station separation distance for both arrays. In other words, the correlation among acceleration spectra reduces with increasing station spacing.

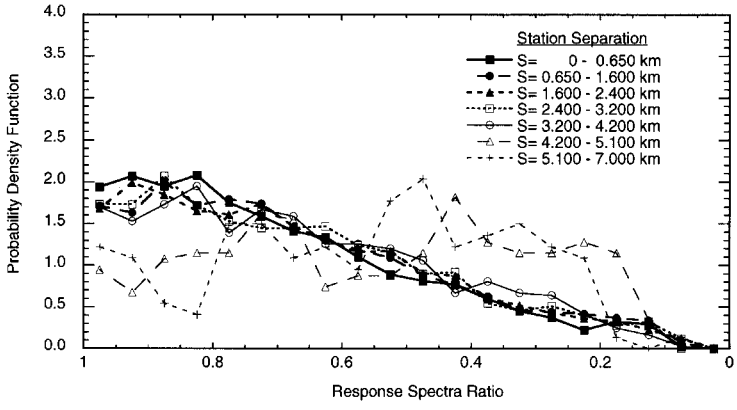

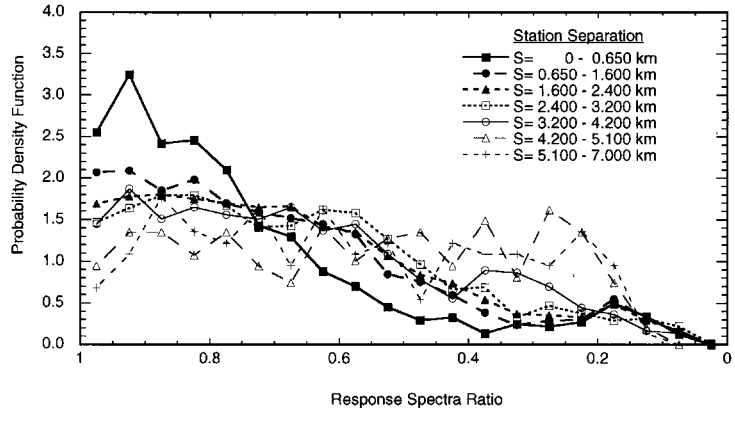

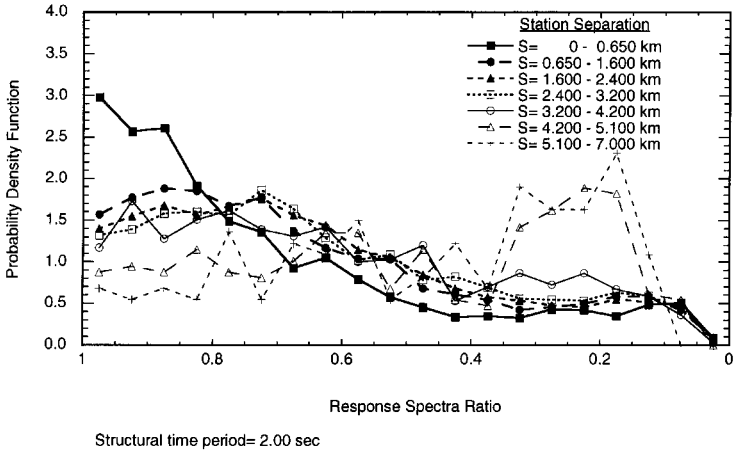

Figure 8. Probability density function for different station separation ranges for SMART-1 array, EW-component, damping = 0·10

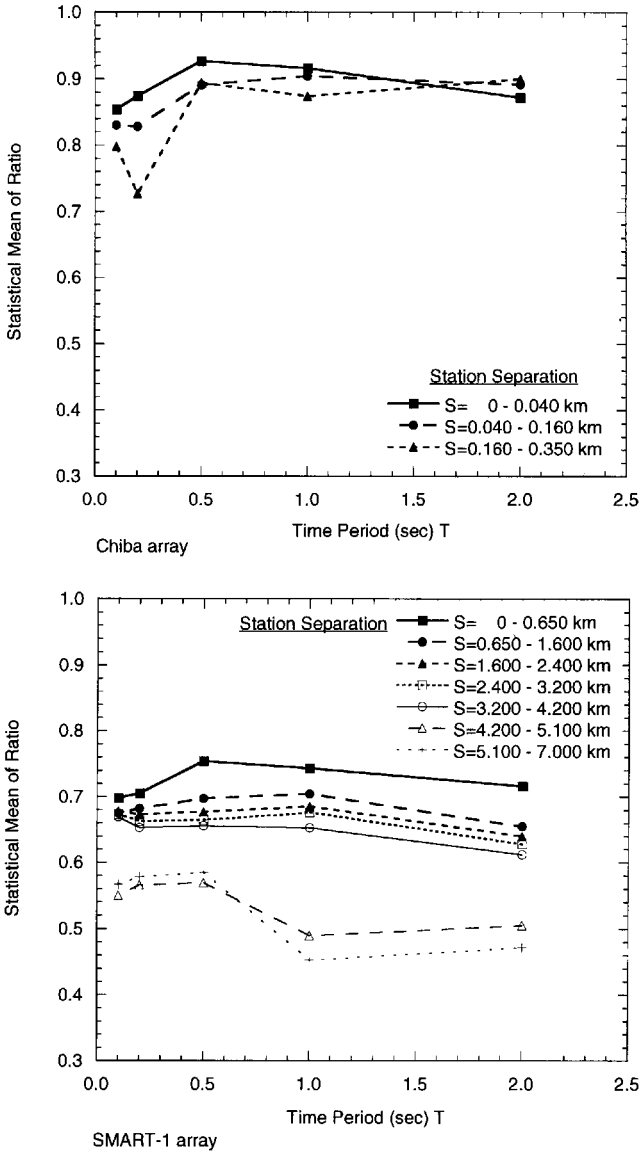

Figure 9(a). Statistical mean of response spectra ratio vs. time period for Chiba array and SMART-1 array, EW-component, damping = 0·10

(2) The correlation among response accelerations at different stations for Chiba array is generally much higher than that for SMART-1 array. The average difference in response spectra between station pairs is 10–20 per cent for Chiba array and 25–50 per cent for SMART-1 array. The response spectra ratio for the shortest station separation range (S = 0–0·650 km) of SMART-1 array shows trends similar to Chiba array although the values are comparatively smaller. This

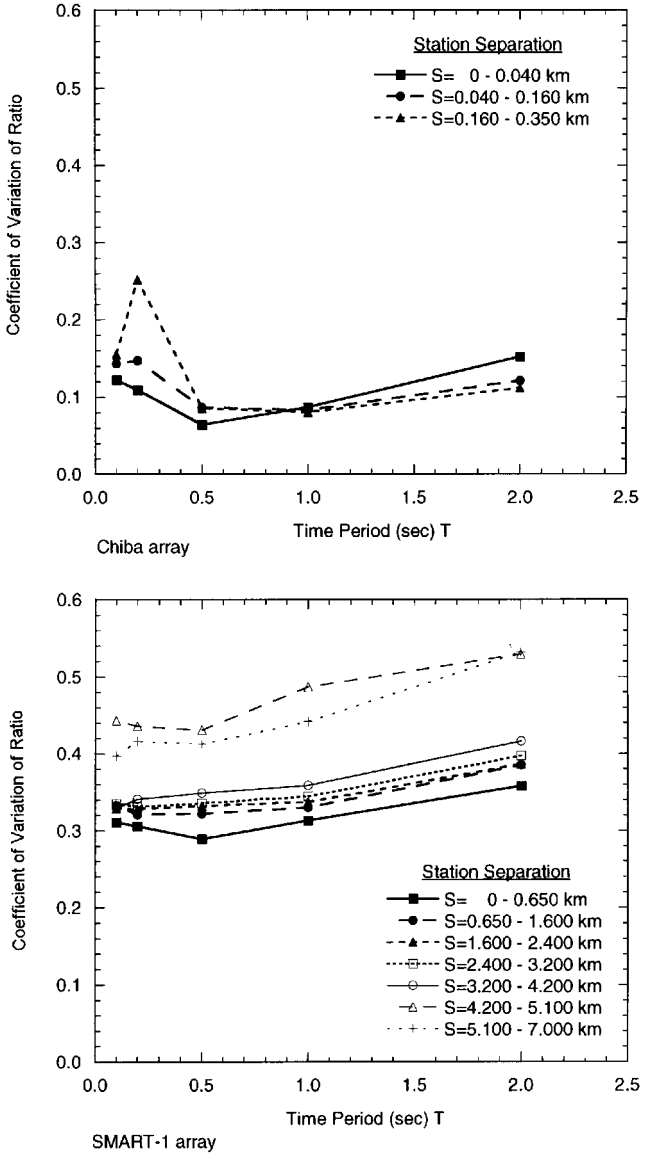

Figure 9(b). Coefficient of variation of response spectra ratio vs. time period for Chiba array and SMART-1 array, EW-component, damping = 0·10

difference persists even when further sub-analysis of SMART-1 data is done by selecting data corresponding to smaller station spacings comparable to Chiba array.

(3) The correlation among response spectra is highest for time periods around 0·5 sec for both arrays. For larger time periods, there is a general decreasing trend in the response spectra ratio with increasing structural time period. On the other hand, a low correlation is observed around

a time period of 0·1–0·2 sec. As seen in Figures 3 and 4 showing the mean of response spectra at each station of the two arrays, this time period range corresponds to the highest peaks in acceleration response spectra for the greater number of records.

(4) Increase in structural damping coefficient results in a small increase in spatial correlation of response spectra. The plots for higher damping ratio value of 0·2 are not being presented in this paper for the sake of brevity.

(5) The coefficients of variation of the response spectra ratio range from 5–25 per cent for Chiba array and 30–50 per cent for SMART-1 array.

5. REGRESSION ANALYSIS

Multiple regression analysis was done separately for the two arrays, Chiba and SMART-1 to observe the influence of the causal factors for the two. To incorporate the effect of qualitative variables like earthquake component and the structural time period, suitable dummy variables have been introduced.

The input data for the regression analysis was generated by calculating ratios of acceleration response spectra for all possible combinations of stations event-wise. Two values of damping ratio, 0·10 and 0·20 were used. The coefficients were then calculated by regression analysis of the data using a least-squares method. A linear relationship between the various variables would be

$$R = a_0 + a_{UD}UD + a_{EW}EW + a_{NS}NS + a_H H + a_M M + a_D D + a_L L + a_{T01}T_{01} + a_{T02}T_{02} + a_{T05}T_{05} + a_{T10}T_{10} + a_{T20}T_{20} + a_S S \quad (1)$$

where, R is the ratio of response spectra, a_0 is the constant term in linear regression equation and a_{UD} to a_S are the coefficients of various variables to be calculated through linear regression. UD, EW and NS are the dummy variables for the qualitative variable earthquake component. H is damping ratio, M is the earthquake magnitude, D is the focal depth of earthquake (km) and L is epicentral distance (km). In any data line T_{01}, T_{02}, T_{05}, T_{10} and T_{20} are the dummy variables for the qualitative variable time period, having a value of 1 for the one relevant structural time period out of the five periods 0·1, 0·2, 0·5, 1·0 and 2·0 sec, and 0 for the other four. S is separation distance for a station pair in km.

However, making both EW and NS equal to 0 simultaneously is a sufficient condition for the vertical component, and also, for the structural time period of 2·0 sec, making the four variables T_{01}–T_{10} equal to 0 is a sufficient condition. Thus, to avoid the perfect multicollinearity problem, the value of coefficients a_{UD} and a_{T20} are assigned the value of 0 as the base category and other coefficients calculated through regression analysis. The coefficients of the other dummy variable terms would then indicate the values with reference to the base category. The regression model is therefore reduced to

$$R = a_0 + a_{EW}EW + a_{NS}NS + a_H H + a_M M + a_D D + a_L L + a_{T01}T_{01} + a_{T02}T_{02} + a_{T05}T_{05} + a_{T10}T_{10} + a_S S \quad (2)$$

The regression analysis was done using full Chiba data, full SMART-1 data and finally a subset of SMART-1 data (station spacings 0·08–0·35 km). For comparing the effect of various parameters,

each of the parameters was normalized by subtracting their mean values and dividing by their standard deviation. The regression equation in its final form is then

$$R = a'_0 + a'_{EW}EW' + a'_{NS}NS' + a'_H H' + a'_M M' + a'_D D' + a'_L L' + a'_{T01}T'_{01} + a'_{T02}T'_{02} + a'_{T05}T'_{05} + a'_{T10}T'_{10} + a'_S S' \tag{3}$$

where the coefficients and normalized parameters are, typically

$$a'_{EW} = (\sigma_{EW} * a_{EW}) \quad \text{and} \quad EW' = \frac{EW - \mu_{EW}}{\sigma_{EW}}, \quad \text{etc}$$

The values of constant term and various coefficients in equation (3) are shown as a summary plot in Figure 10 with the error bars indicating the standard regression error for each parameter. We observe that:

(1) The coefficient of station spacing S' is negative for all the three cases. Since lower values of ratio R indicate lower correlation, negative signs of coefficients again indicate reduced correlation with increasing station spacing.

(2) The coefficient for T'_{05} (0·5 sec) is positive for all cases and is also the largest among the time period coefficients, indicating the highest correlation among the time periods considered.

The coefficient for time periods T'_{20} (2·0 sec) being assumed zero as base, is the lowest for SMART-1 array. For Chiba array, coefficients of T'_{01} and T'_{02}, being negative, are the lowest.

(3) The coefficient for the UD component normalized parameter UD' having been assumed to be 0 as base, the coefficients for the horizontal earthquake component parameters EW' and NS', are positive for Chiba array as well as both the cases of SMART-1 array. This indicates a lower

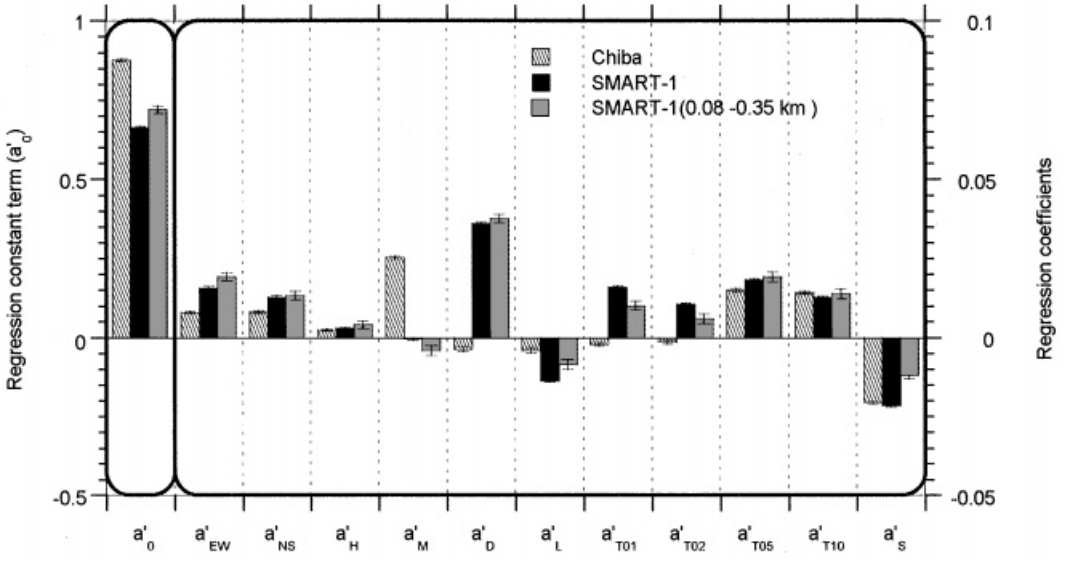

Figure 10. Summary plot for regression equation coefficients with error bars showing standard error of regression

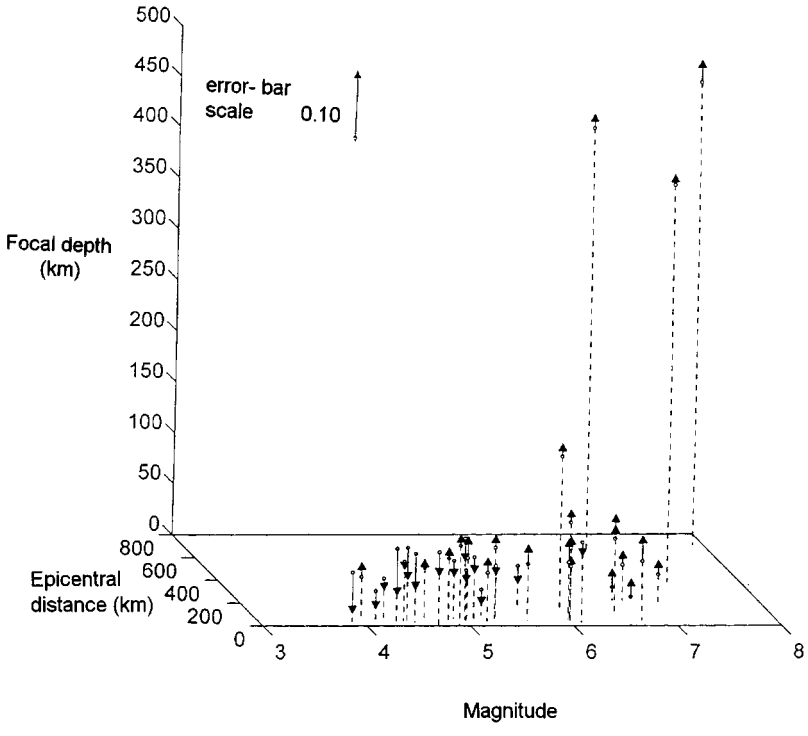

Figure 11. Chiba array-effect of earthquake magnitude (M), focal depth (D) and epicentral distance (L)

correlation of response spectra for the vertical component compared to the horizontal components in all cases considered.

(4) The coefficient for damping term is positive for all the cases, indicating increase in correlation of response acceleration among stations with increase in damping ratio.

(5) From a first look at the values of regression coefficients in Figure 10, the effects of the earthquake magnitude, focal depth and epicentral distance appear to be complicated. The scatter plots of focal depth vs. epicentral distance and vs. hypocentral distance for the two arrays shown in Figures 11 and 12 indicate the differences in the inter dependence and variance of the three parameters among the two arrays:

(a) For Chiba array, majority (24 of total 39) of the events have focal depth of the order of 60 km and epicentral distance of the order of 50 km. Except for two events, all the Chiba events have hypocentral distance larger than 60 km.

(b) For SMART-1 array, a majority of events (22 of total 40 and accounting for 66 per cent of the regression data) have focal depth of the order of 10 km and epicentral distance of the order of 40 km. The hypocentral distance for all these events is less than 50 km. The SMART-1 data therefore mainly consist of shallow, near-source events.

(c) Large magnitude earthquakes have large focal depths and epicentral distances for the records of both the arrays.

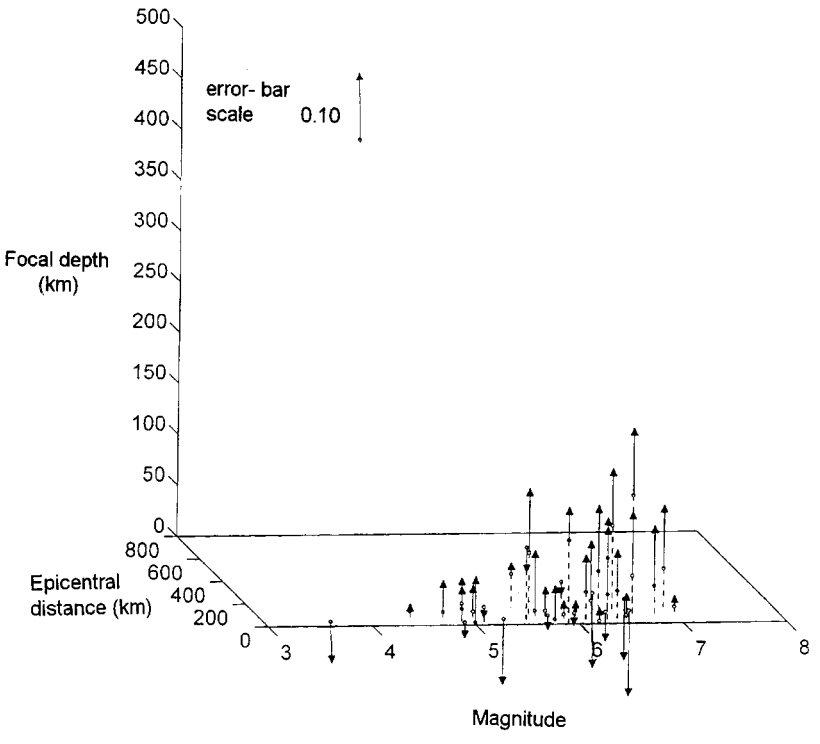

Figure 12. SMART-1 array-effect of earthquake magnitude (M), focal depth (D) and epicentral distance (L)

To understand the combined effect due to the parameters M, L and D, we calculated the difference between the actual response spectra ratio and that calculated by the regression equation, excluding the terms corresponding to these three parameters for each event. These values are shown as error bars in the three dimensional plots shown in Figure 11 for Chiba array and Figure 12 for SMART-1 array where the three axes correspond to the event properties, magnitude, focal depth and epicentral distance. The upward direction of error bar arrow indicates positive sign of the contribution and downward, negative. It may be noted that the number of positive values of error bar need not match the number of negative error bars inspite of parameters being normalised in equation (3) since the number of stations triggered in different events is unequal and has an effect of weighting the data.

As can be observed from the Figures 11 and 12, the three parameters having an inter dependence, their combined effect shows a positive contribution to the value of ratio of response spectra with an increase in magnitude, epicentral distance or focal depth in the case of large scale earthquakes.

5.1. Effect of damping ratio and time period

For considering the effect of the damping ratio and time period terms, plots of acceleration spectra ratio vs. station separation were drawn for Chiba as well as SMART-1 array, for each of

the three earthquake components. For comparison, a standard case was assumed with parameter values as

$$H = 0{\cdot}1, \quad \mathrm{M} = 5, \quad \mathrm{D} = 50\ \mathrm{km}, \quad \text{and} \quad L = 50\ \mathrm{km}$$

$$T_{01} = 0, \quad T_{02} = 0, \quad T_{05} = 1, \quad T_{10} = 0$$

Then, for considering the qualitative effect of structural time period, the dummy variable values for T_{01}–T_{10} were changed for each case. For considering the quantitative effect of damping ratio, the values were taken as

$$H = 0{\cdot}1, 0{\cdot}2$$

Since the ratios of accelaration response spectra at each station were calculated using dummy variables for the three components, the regression equation reflects the overall characteristics of all the three components. For our discussion, we consider the case of EW component for both the arrays.

The effect of damping and time period on the ratio of acceleration response spectra is shown in Figure 13 for Chiba array, SMART-1 array and the subset of SMART-1 array with station spacing less than 0·35 km. Keeping in mind that higher values of spectral ratio indicate higher correlation, we find that:

(1) An inverse relationship between response spectra ratio and station separation is evident from all the curves. It may be noted that the scale of station separation axis is different for different cases. The slope of spectral ratio vs. station separation line is considerably steeper for Chiba array than the slope of the regression relation obtained in case of SMART-1 array. However, when only the data in the station spacing range (0·08–0·35 km) is considered for SMART-1 array, the slope of the line is of the order of the slope for Chiba array case. The absolute values of ratio of peak response acceleration are also generally higher when this smaller station separation data set is used, indicating a comparatively more uniform response when considering smaller station separations.

(2) In general, the ratio of response spectra even for comparable station spacings is appreciably lower for SMART-1 array compared to that for Chiba array. Site specific effects may be responsible for the difference.

(3) The variation of acceleration spectra shows frequency dependence. In qualitative terms, the response spectra ratio shows a low for 0·1–0·2 sec time periods and high for 0·5 sec. Beyond 0·5 sec, the ratio shows a general downtrend with increasing time period for 1·0 and 2·0 sec periods.

(4) The response spectra ratio increases with increase in structural damping.

6. CONCLUSIONS

Considering all the three earthquake components, 1338 free field strong motion records from Chiba array in Japan and 2917 records from SMART-1 in Taiwan have been analysed. The ratio of acceleration response spectra ordinates has been used as a measure of variation in the response between any two stations. Between 0 and 1, a larger value of ratio is indicative of lesser variation.

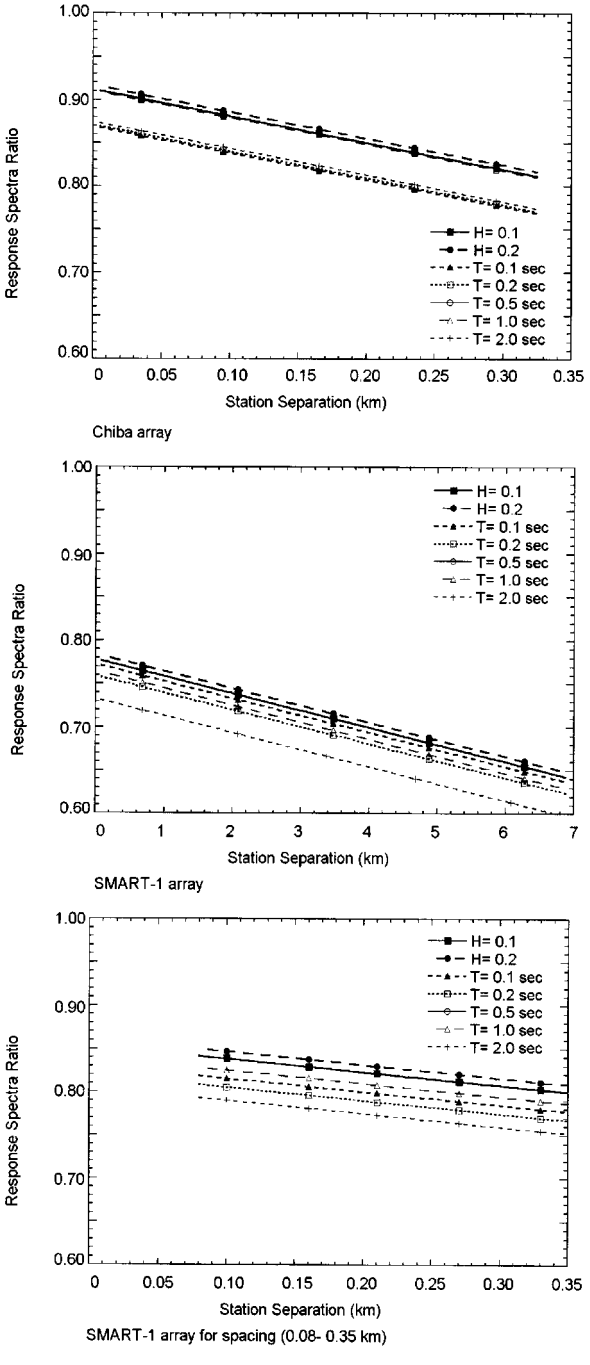

Figure 13. Regression equation plots for EW-component of Chiba array, SMART-1 array full data and SMART-1 data subset with station separation less than 0·35 km

The following conclusions are drawn:

(1) A very large scatter of the response spectra ratio is observed for both arrays, especially for SMART-1 array. In general, the mean values of the ratio range from 10 to 20 per cent for Chiba array while they range from 25 to 50 per cent for SMART-1 array. The coefficients of variation of the ratio vary from 5 to 25 per cent for Chiba array and 30–50 per cent for SMART-1 array. The primary factor responsible for the values of response spectra ratio is shown to be station separation. However, its physical interpretation is difficult to make on this scatter and the governing mechanism producing the degree of variations remains for future study. There appears to be effects of space variation in local geophysical conditions, directional variation in radiation wave patterns from earthquake sources, and path differences.

(2) The probability density function of response spectra ratio is frequency dependent. The high peaks near the higher ratio end reflect the higher correlation among response spectra in statistical terms. The highest peaks are observed for time periods around 0·5 sec. For SMART-1 array, the frequency dependence for the shortest station separation range ($S = 0$–$0{\cdot}650$ km) shows general trends similar to Chiba array although the peaks are lower. Larger station separation as well as site specific characteristics appear to contribute to the difference.

(3) The response spectra ratio reduces with increased station separation but the slope of the plot indicating rate of reduction is much lower for full SMART-1 data. The spatial variation trend of response spectra for SMART-1 data subset (for spacing = 0·08–0·35 km) is similar to the plots for Chiba array with comparable spacings. The values of ratio for the subset are also higher compared to full SMART-1 data case. The changes in values and trend for the SMART-1 data subset reflect the effects of reduced station separation.

(4) The correlation in response acceleration shows a low around 0·1–0·2 sec and is highest for time periods around 0·5 sec. Beyond this, the ratio shows a general downtrend with increasing time period for 1·0 and 2·0 sec periods.

(5) The correlation among response spectra is lower for UD component as compared to the horizontal components. The regression coefficients for *NS* and *EW* component parameters are positive and nearly equal for both the arrays, indicating nearly equal correlation in the two directions.

(6) The effect of earthquake magnitude, focal depth and epicentral distance on the spatial variation is complex. The three parameters having implicit interdependence, considering their combined effect, a positive contribution to the value of ratio of response spectra is observed in case of larger earthquake events.

(7) Higher damping ratio results in higher correlation of response spectra.

ACKNOWLEDGEMENTS

The authors wish to thank the Association for Earthquake Disaster Prevention of Japan and National Geophysical Data Center in U.S.A. for publishing the strong motion array record database and the University of Tokyo for providing the strong motion records.

REFERENCES

1. T. Katayama, F. Yamazaki, S. Nagata, L. Lu and T. Turker, 'Development of strong motion database for the Chiba seismometer array', *Report* No. 90-1 (14), Earthquake Disaster Mitigation Engineering, Institute of Industrial Science, University of Tokyo, 1990.
2. T. Katayama, F. Yamazaki, S. Nagata, L. Lu and T. Turker, 'A strong motion database for the Chiba seismometer array and its engineering analysis', *Earthquake Engng. Struct. Dyn.* **19**, 1089–1106 (1990).

3. B. A. Bolt, C. H. Loh, J. Penzien, Y. B. Tsai and Y. T. Yeh, 'Preliminary report on the SMART-1 strong motion array in Taiwan', *Report* No. UCB/EERC-82/13, Earthquake Engineering Research Center, University of California, Berkeley, CA, 1982.
4. I. A. Beresnev, K. L. Wen and Y. T. Yeh, 'Source, path and site effects on dominant frequency and spatial variation of strong ground motion recorded by SMART-1 and SMART-2 arrays in Taiwan', *Earthquake Engng. Struct. Dyn.* **23**, 583–597 (1994).
5. K. L. Wen and Y. T. Yeh, 'Seismic velocity structure beneath the SMART-1 array', *Bull. Inst. Earth Sci. Acad. Sinica* **4**, 51–72 (1984).
6. K. L. Wen and Y. T. Yeh, 'Array analysis of site effects on strong ground motions', XIX IUGG Assembly, IASPEI/IAEE Joint Workshop, Vancouver, 1987.
7. Magnetic Tapes No. SM-TAI01, SM-TAI02, SM-TAI03, SM-TAI04, National Geophysical Data Center Archive, U.S.A.
8. J. F. Schneider, J. C. Stepp and N. A. Abrahamson, 'The spatial variation of earthquake ground motion and effects of local site', *Proc. Earthquake Engng. 10th World Conf.*, Madrid, Spain, 1992, pp. 967–972.
9. Database Advisory Committee and Working Sub-committee, 'Strong motion array record database-data manual', Association for Earthquake Disaster Prevention of Japan, Vol. A01, July 1992.

